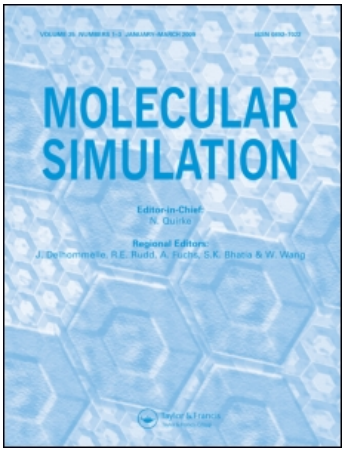

Molecular Simulation
Publication details, including instructions for authors and subscription information:
http://www.informaworld.com/smpp/title~content=t713644482

Experimental and Simulation Studies of Electro-rheology

P. Bailey[a]; D. G. Gillies[a]; D. M. Heyes[a]; L. H. Sutcliffe[a]
[a] Department of Chemistry, Royal Holloway and Bedford New College, University of London, Surrey, UK

To cite this Article Bailey, P. , Gillies, D. G. , Heyes, D. M. and Sutcliffe, L. H.(1989) 'Experimental and Simulation Studies of Electro-rheology', Molecular Simulation, 4: 1, 137 — 151
To link to this Article: DOI: 10.1080/08927028908021970
URL: http://dx.doi.org/10.1080/08927028908021970

Molecular Simulation, 1989, Vol. 4, pp. 137–151
Reprints available directly from the publisher
Photocopying permitted by license only

EXPERIMENTAL AND SIMULATION STUDIES OF ELECTRO-RHEOLOGY

P. BAILEY, D.G. GILLIES, D.M. HEYES and L.H. SUTCLIFFE

Department of Chemistry, Royal Holloway and Bedford New College, University of London, Egham, Surrey TW20 0EX, UK.

(*Received January 1989, accepted January 1989*)

Electro-rheological fluids are colloidal dispersions that, under the influence of an applied electric field, can show a spectacular increase in yield stress and viscosity. Despite many technological roles for fluids with a viscosity that can be controlled electrically, progress at making them commercially viable products has been slow, partly due to a lack of understanding of this phenomenon at the microscopic level. In this report, simulation and experimental data are combined to provide insights into the microscopic origins of this effect. The simulations produce electric field-induced 'strings' of particles that span the electrodes, in agreement with the experimental observation, and are responsible for the major enhancements in the viscosity. The field also causes a strong distortion in the first coordination shell of colloidal particles. The combination of shear and electric field produces a long-range microstructure that is periodically forming and decaying, caused by the competing effects of electric field and shear rate. Comparison with experiment reveals that the Electro-rheological effect is driven by the applied field-induced Stokesian diffusion of the solid particles and relies little on the accompanying Brownian motion.

KEY WORDS: Electro-rheology, Brownian dynamics, viscosity

1. INTRODUCTION

It has been known for over 40 years that when certain particles, dispersed in an insulating liquid, are subjected to electric fields of several $kV\,mm^{-1}$, a marked increase in the macroscopic viscosity is observed. This is called the electrorheological (ER) effect. Winslow [1] was a pioneer in this area, having identified a number of the important factors optimising the ER effect. He found that moist silica gel particles of $\sim 1\ \mu m$ diameter, σ, suspended in kerosene at a volume concentration of $\sim 50\%$ had a strong ER effect. He noted that the particles migrate to form chains along the field lines between the plates, which are also used for shearing the entrained suspension. A recent observation of this field-induced percolation transition is given in ref. [2]. Since then progress has been slow despite the incentive of obvious applications of the effect in, for example, suspension devices, shock absorbers, clutches and brakes. Klass and Martinek [3, 4] showed that the ER effect increases with electric field strength, temperature and decrease in frequency of an applied AC electric field. Block et al. demonstrated a shear rate dependence of the dielectric properties [5]. As part of the RHBNC Chemistry Functional Fluids Group we have been performing rheological measurements, esr and nmr experiments on ER fluids and Brownian Dynamics (BD) simulations of these materials to characterise and understand them better. In Figure 1 we show a typical example (produced in our laboratory using a specially instrumented electroviscometer) of the increase in viscosity with electric field of a LiPMA particulate dispersion in silicone oil [6]. The electric field increases linearly with time and is then turned off suddenly. This sequence is repeated several times to test for

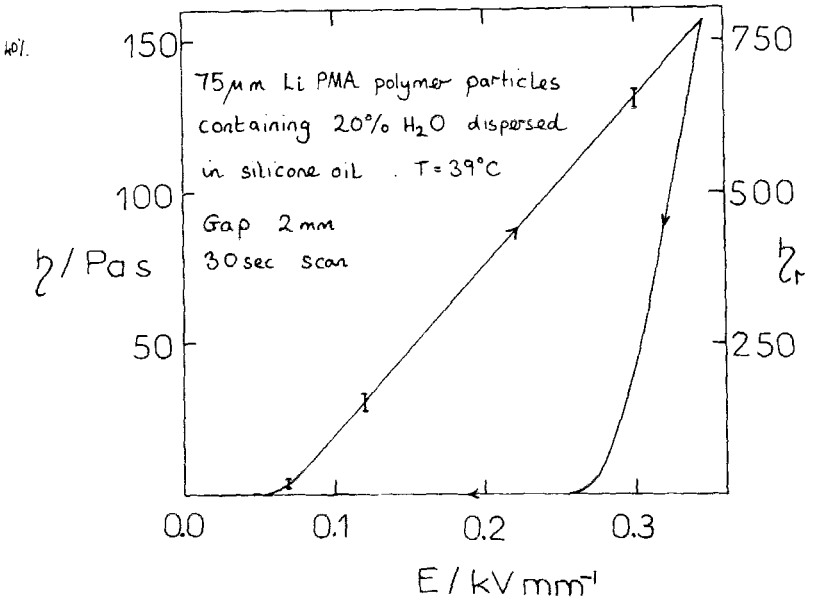

Figure 1 The viscosity of a LiPMA polymer suspension in silcone oil at a volume fraction of 25%. The polymer contains 20% water is sheared at $\dot{\gamma} = 1\,s^{-1}$. The applied voltage is increased at a uniform rate for 30 *s* and then turned off. The viscosity of the oil is 2 cPas. $\eta_r = 5$ for $E = 0$. The electric field, E, is applied across a 2 mm gap. At the top of the η vs E curve, the voltage is suddenly turned off. The direction of the cycle is denoted by the arrows. The cycle is repeated several times with no evidence of hysteresis. Bars are given on the figure to indicate the spread of rise curves.

hysteresis. The particles range between 50–100 μm in diameter. The volume fraction of solids is 25%. The field-off relative viscosity of the dispersion is 5–10. The pure oil has a viscosity of 2 cPas at 298 *K*. The viscosity is measured at a shear rate of $1\,s^{-1}$. The slow build-up of viscosity during ascending field and more rapid decay of viscosity on turning off the field is indicative of some form of field-induced structural change. A similar effect is observed when dense fluids are sheared in the shear-thinning regime. Stress over-shoot is also observed when the field is suddenly ramped to a large value at fixed shear rate [6, 7]. In this report we describe the first application of molecular simulation to the ER effect to gain insights into its molecular origins.

2. THEORY AND SIMULATION METHOD

In these simulations we generate the positions of model colloidal particles subject to an electric field in the y direction and to laminar shear flow, dv_x/dy. The molecular configurations are generated at fixed time intervals, h, using the Brownian Dynamics, BD, technique [8]. First we will describe the basics of BD and then the method of including the electric field and shear.

The Strict Langevin BD method employed here has been fully described elsewhere [8]. It treats the suspending medium on two independent levels. The background fluid acts to dampen out the velocities of the colloidal particles. The force on the particles

by the solvent opposes the velocity through a friction coefficient, β. The discrete nature of the solvent is taken into account by a random force R acting upon the colloidal particles. The value of the random force on each particle changes with time in order to represent the net effect of the collisions of the solvent molecules on the colloidal particle. In each time interval there is an imbalance on either side of the colloidal particle, leading to the net force, R. This represents the net effect of the suspending medium over a fixed time interval (i.e., h).

$$\ddot{r} = F/m + R/m - \beta\dot{r} \tag{1}$$

where r is the position of an arbitrary macromolecule, F is the systematic component of the force derived from the pair interactions between the colloidal particles and m is the mass of the colloidal particle (assumed all the same here). The algorithm for updating the particle positions is,

$$r_x(t + h) = r_x(t) + (F(t) + R_x(t, h))\, h/m\beta + \gamma r_y(t). \tag{2}$$

$$r_y(t + h) = r_y(t) + (F_y(t) + R_y(t, h))h/m\beta, \tag{3}$$

$$r_z(t + h) = r_z(t) + (F_z(t) + R_z(t, h)h/m\beta, \tag{4}$$

where γ is the applied shear rate. Sliding (Lees-Edwards) boundary conditions are employed at the BD cell boundaries to maintain continuity of shear velocity profile across all space [8]. The random force is taken from a normal distribution with standard deviation, $\langle R_\alpha^2(t, h)\rangle$, where,

$$\langle R_a^2(t, h)\rangle = 2mk_B T\beta/h, \tag{5}$$

where $\alpha = x$, y or z. The colloid–colloid particle potential, $\phi(r)$, has the form,

$$\phi(r_{ij}) = \varepsilon(\sigma/r_{ij})^{12} + (\mu_y^2/r_{ij}^3)(1 - 3r_{yij}^2/r_{ij}^2), \tag{6}$$

where the first term represents the core–core repulsion and is called the soft-sphere potential. The y component of the separation between particles i and j, r_{ij}, is r_{yij}. The second term is, to first order, the intermolecular interaction due to the external field induced dipoles, μ_y. Therefore,

$$F_x = 12(r_{xij}/r_{ij})\varepsilon\sigma^{12}/r_{ij}^{13} + 3\mu_y^2(r_{xij}/r_{ij}^5)(1 - 3r_{yij}^2/r_{ij}^2) - 6(\mu_y^2/r_{ij}^3)(r_{xij}r_{yij}^2/r_{rij}^4), \tag{7}$$

$$F_y = 12(r_{yij}/r_{ij})\varepsilon\sigma^{12}/r_{ij}^{13} + 3\mu_y^2(r_{yij}/r_{ij}^5)(1 - 3r_{yij}^2/r_{ij}^2) + 6(\mu_y^2/r_{ij}^3)(r_{yij}/r_{ij}^2 - r_{yij}^3/r_{ij}^4), \tag{8}$$

$$F_z = 12(r_{zij}/r_{ij})\varepsilon\sigma^{12}/r_{ij}^{13} + 3\mu_y^2(r_{zij}/r_{ij}^5)(1 - 3r_{yij}^2/r_{ij}^2) - 6(\mu_y^2/r_{ij}^3)(r_{zij}r_{yij}^2/r_{ij}^4), \tag{9}$$

The BD simulations were performed on a cubic unit cell of volume V containing $N = 108$ macroparticles. To help establish scaling relationships, the calculations were performed in reduced units, i.e., $k_B T/\varepsilon \to T$, and number density, $\varrho = N\sigma^3/V$. Time is in $\sigma(m/\varepsilon)^{1/2}$, shear rate is in $(\varepsilon/m)^{1/2}/\sigma$, viscosity is in $(m\varepsilon)^{1/2}/\sigma^2$ and stress is in $\varepsilon\sigma^{-3}$. Calculated quantities are mostly given in terms of these units. The effective hard-sphere diameter, σ_{HS}/σ, of the soft-sphere potential is [9],

$$\sigma_{HS}/\sigma = 0.9359/T^{12}, \tag{10}$$

The fluid density of the hard-sphere fluid at fluid-solid coexistance is, $\varrho_{HS} = 0.9428\, N\sigma_{HS}^3/V$. Therefore, the coexistence fluid density in soft-sphere units is

1.15[10]. The simulations reported here were conducted at $\varrho = 0.6$, $\varepsilon = 298\,k_B$ and $T = 1.0$. The solids volume fraction is $\phi = (\pi/6)\varrho_{HS}$, where ϱ_{HS}, where $\varrho_{HS} = (0.9359)^3\varrho = 0.492$, hence $\phi = 0.26$, which is close to the experimental value. Other material parameters were chosen to be the same as those of the experimental system considered in Figure 1. The density of the solvent and particles was $960\,kg\,m^{-3}$, the viscosity of the suspending fluid (0.02 Pas), the temperature (298 K) and the size of the particle was $\sigma = 75\,\mu m$.

It is still not known what the precise effect of the external field is on the colloidal particles. We have modelled its effect as an induced point dipole at the centre of each macromolecule which at all time, while the field is applied, points along the direction of the field (i.e., y, here). When the field is 'turned-off' the dipole moment is set to zero. We have deliberately kept the model as simple as possible in this preliminary study, in order to establish the minimum microscopic requirements for the ER effect. The value of this dipole moment, μ_y, that produced a strong ER effect in the simulations was 4.0 in reduced units. This is reasonable because experience gained in simulations of other non-Newtonian phenomena (e.g., shear thinning and thickening) has revealed that a close competition between the hard-core repulsions and the perturbing force is required to produce these effects [11]. For the dipolar interactions to compete successfully with the short range repulsions the coefficient of the dipolar interaction must be of order unity in reduced units. Assuming that the point dipole is E/α where E is the electric field and α is the polarizability then we can relate the reduced point dipole in the simulation, μ_y^*, to E. In fact, $E = \mu_y^*(4\pi\varepsilon_0\varepsilon_r\varepsilon\sigma^3)^{1/2}/(\alpha' 4\pi\varepsilon_0)$, where α' is polarizability volume ($=\sigma^3$). For $\mu_y^* = 4$ used in these simulations then the electric field is, $75\,V/m$ (choosing the relative permittivity $\varepsilon_r = 4$), compared with typical values employed experimentally ($\sim 10^6$ V/m). We suggest that an experimentally applied electric field is severely attenuated by the suspending medium by an unknown mechanism, which is probably beyond the level of approximation of the present model. The point dipole model is clearly a simplification but it is not possible at present to be more definite as to the charge reorganisation caused by the applied electric field.

There are a number of time-scales associated with this system of particles in a hydrodynamic background medium which for many applications of colloidal dispersions are helpful in interpreting the observed effects [8]. The macroparticles themselves have an 'inherent' time-scale for structural relaxation, τ_k, in the absence of the solvent which would be important if the particles were to move in a vacuum,

$$\tau_k = \sigma(m/\varepsilon)^{1/2} \tag{11}$$

where ε is a characteristic energy of interaction such as a pair potential well-depth. There is the time scale for velocity fluctuations of the macromolecule to decay, $\tau_p = \beta^{-1}$,

$$\tau_p = m/3\pi\sigma\eta_s, \tag{12}$$

where η_s is the viscosity of the pure suspending medium. There is also the time scale for local structural organisation, τ_r, the time it takes a molecule to diffuse $\sigma/2$ at extreme dilution.

$$\tau_r = 3\pi\sigma^3\eta_s/4k_BT, \tag{13}$$

The time step was 33 reduced time units or 966s. The $\tau_p = 0.45$ s and $\tau_r = 4.8 \times 10^6$ s. The intrinsic time scale for significant movement of these particles in suspension is therefore very long even on human time scales. We consider reduced

shear rates in terms of the Peclet number, $P_e = \tau_r \gamma/2$, of order unity.

Just as we use an effective electric field many orders of magnitude smaller than the experimental values, similarly, we used shear rates many orders of magnitude smaller than the experimental value ($\sim 1\,s^{-1}$). The particles modelled are 75 μm in diameter, substitution of this value and the other system parameters described above in equation (13) yields a structural relaxation time, τ_r, equal to 4.8×10^6s or for the experimental shear rate of $\gamma = 1\,s^{-1}$ a Peclet number, $P_e = 2 \times 10^6$. This is enormous compared with typical previous rheological studies [8], where $P_e \leqslant 100$. Present Brownian Dynamics cannot operate stably at this high P_e at present. The latter we attribute to the inadequacies of Strict Langevin BD, which fails to account for the true many body hydrodynamic effects that dominate when colloidal particles approach closely. The background medium should slow down the approaching colloidal particles and damp out close encounters. This complicated many-body effect is not incorporated within the present model. This causes the simulated collisions to take place too quickly and be too severe within the driving force of the local potential surface. We consider that the lower shear rates considered here produce states which correspond approximately to those produced at higher shear rates in the real experimental systems. This is because the colloidal particle collisions will be of a severity and proximity appropriate to a much higher shear rate than that used in the simulations. For the same reason, we find the shear rates of experimental magnitude are not stable when employed in a simulation because the collisions become too fierce, causing the algorithm to fail. Although the shear rates in the simulation are smaller than in the experiments, we suggest that they produce similar states. Computation were carried out on a VAX 11/780 at the Royal Holloway & Bedford New College Computer Centre.

3. RESULTS AND DISCUSSION

The simulations were carried out in 500 time-step subaverages. Over 800 subaverages were made with the system subjected to a range of shear rates and applied electric fields. The shear viscosity of the suspension, η, is related to the viscosity of the background fluid, η_s, as follows.

$$P_{xy} = -\frac{1}{V}\sum_{i=1}^{N-1}\sum_{j\neq i}^{N} r_{xij} r_{yij} \frac{d\phi}{dr}/(2r_{ij}), \tag{14}$$

where V is the (cubic) volume containing the N particles and where r_{xij} is the x component of the separation between particles i and j, r_{ij},

$$\eta = -P_{xy}/\gamma. \tag{15}$$

The relative viscosity, η_r is defined as,

$$\eta_r = 1 + \eta/\eta_s. \tag{16}$$

In Figure 2 we present the relative viscosities, η_r, for the considered system (N = 108) against run number. The shear rates (P_e) employed are given in the insert. All subaverages were conducted with $\mu_y = 4$, except for a short block around NRUN = 600, where $\mu_y = 0$, again marked on the figure. The low shear rate states have high viscosities. The states $P_e = 0.02$ and 0.05 are particularly pronounced in

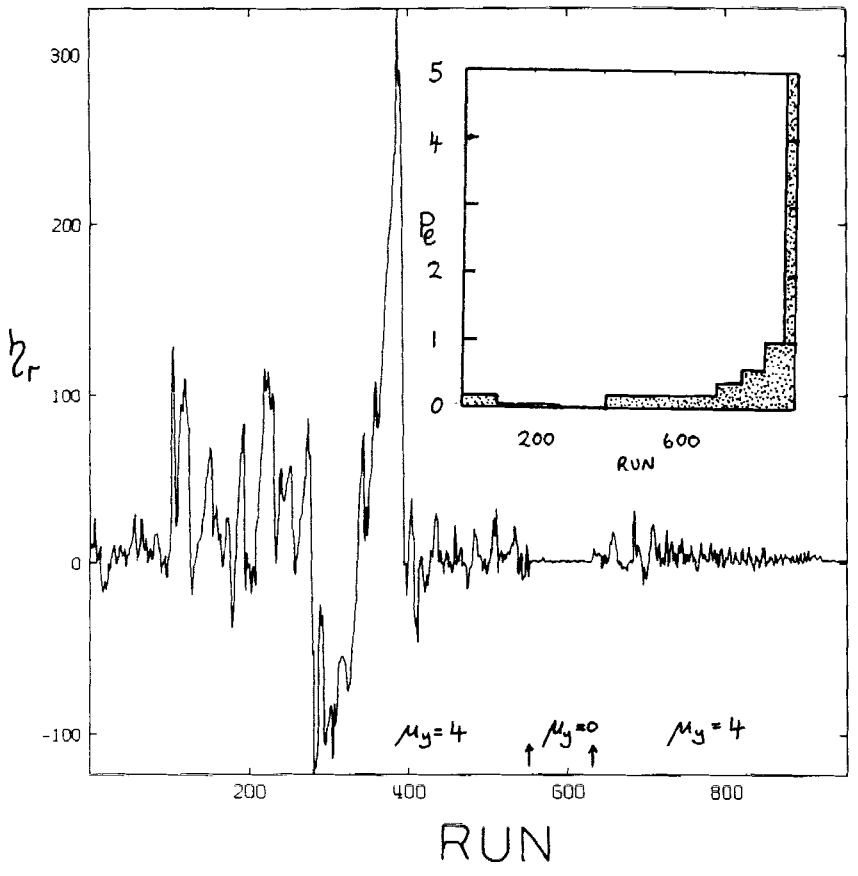

Figure 2 The relative viscosity, η_r averaged over each subaverage. The insert gives the P_e over the same sequence. The dipole moments are also indicated along the base-line.

this respect, manifesting large fluctuations in viscosity. It is possible for the shear viscosity to go temporarily negative because a very small number of molecules is considered. Structural changes in the fluid, especially following a drop in P_e, can give rise to a positive P_{xy} and hence a negative viscosity. This is noticeable for NRUN $\approx$ 300 just after P_e 0.05 $\rightarrow$ 0.02. When the electric field is turned off around NRUN = 600 the viscosity does not manifest the large fluctuations evident at the same shear rate (P_e = 0.2) with the field on. As there is often a close relationship between structure and stress, this indicates that the associated structural fluctuations vary similarly. Table 1 reveals that the ER effect increases with electric field, as observed in experiment.

The osmotic pressure, P, of the system is,

$$P = -(1/6V)\left(\sum_{i}^{N-1}\sum_{j\neq i}^{N} r_{ij}\frac{d\phi(r)}{dr}\right). \tag{17}$$

Table 1 Properties averaged over subaverages with the same μ_x and P_e. $\varrho = 0.6$ and $T = 1$, $A = P_{xx} - P_{yy}$ and $B = P_{yy} - P_{zz}$. NR is the number of subaverages.

NR	μ_y	P_e	A	B	P	η_r
3	4	0.00	−17.19	12.38	7.14	9.91
99	4	0.20	−19.33	16.47	9.24	5.51
178	4	0.05	−13.36	11.42	7.95	37.96
131	4	0.02	−19.63	18.40	10.30	27.52
139	4	0.20	−20.39	18.11	9.85	4.02
80	0	0.20	−0.13	0.14	2.91	1.28
98	4	0.20	−18.55	16.37	9.26	5.38
70	4	0.40	−18.08	14.63	8.22	4.45
67	4	0.60	−23.75	20.99	10.39	2.83
55	4	1.00	−23.89	22.15	11.01	3.32
29	0	0.20	−0.15	0.25	2.84	1.14
57	0.5	0.2	−0.38	0.40	2.85	1.30
107	0.5	0.05	−0.35	0.36	2.86	1.53
63	1.0	0.05	−1.30	1.30	2.84	1.25
89	1.5	0.05	−2.88	2.87	2.98	1.48
111	2.5	0.05	−7.71	7.70	4.69	2.70
165	3.5	0.05	−11.69	10.96	7.21	14.1

We have monitored, P, during these sequence of runs and give it in Figure 3. The regime of negative viscosity corresponds to a rise in pressure. The shear-free runs manifest a low pressure with small fluctuations. The normal pressure components, P_{xx}, P_{yy} and P_{zz} were evaluated,

$$P_{xx} = -\frac{1}{V}\sum_{i=1}^{N-1}\sum_{j\neq i}^{N} r_{xij}r_{xij}\frac{d\phi}{dr}\Big/(2r_{ij}), \tag{18}$$

with obvious changes for the y and z components. In Figure 4, $P_{xx} - P_{yy}$, is given. The sign is in accordance with that found for non-newtonian fluids [8]. In absolute terms, for particles of this size 100 reduced pressure units is equivalent to 10^{-11} bar of pressure. Therefore the electric field is pushing the plates apart with insignificant pressure even though the electric field causes some major extra dense packing of the macroparticles between the shearing/electrode plates. The quantity, $P_{yy} - P_{zz}$, shown in Figure 5 has a sign typical of non-Newtonian fluids but again of a dramatically increased magnitude.

These physical properties are what one would expect from the observed structural changes in the fluid. The field aligns the particles into bands or 'strings' along the field lines. Monte Carlo simulations of hard core magnets has reealed a similar aggregating influence of a 'dipolar' term in the intermolecular potential [12]. Figure 6 shows this effect as a projection of molecular centres on the faces of the BD cell. Image BD cells are also shown to facilitate perception of the long range order forming, which can span the cells. The Peclet number is 0.02. There are regions of high density and low density that alternate in the shear (xy) plane. These strings are of approximately one molecule in diameter, when viewed in plane of the electrode (xz). They are continually being formed (perpendicular to the plates). They then tilt in the x direction become taut and then break up. Figure 6(c) shows one string in the latter stages of this process. The stress from each string maximises just before it breaks up. These strings should not be confused with those formed along the streaming direction for monatomic fluids [11].

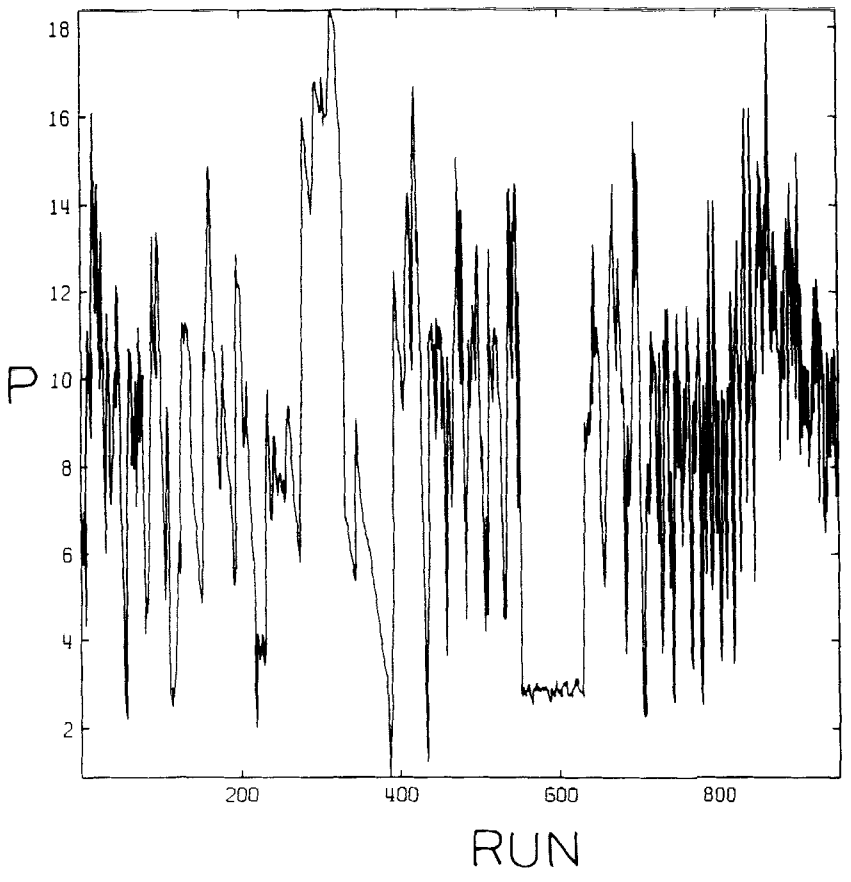

Figure 3 As for Figure 2 except the pressure, P, is given over the same sequence.

In Figure 7, we show a field-on state at the higher shear rate of $P_e = 0.05$. The strings are caught in a largely slanting disposition. They are again well-ordered in the forward (yz) plane. Figure 8 gives the equivalent pictures for $P_e = 0.2$. Figure 9 presents similar plots for $P_e = 0.4$. As the shear rate steadily increases through this sequence of figures we not that arbitrarily chosen 'snapshots' of the fluid reveal strings in ever increasingly slanted aspects (see e.g., Figure 9(c)). As shear rate rises precipitously to $P_e = 5$ we observe that the strings themselves align to form xy planes (Figure 10). The shear flow is beginning to dominate over the electric field and the particles are starting to adopt phases reminiscent of those observed in laminar flow of monatomic fluids [11].

The short range structure of these electrified fluids is discerned through the pair radial distribution function, $g(r)$,

$$g(r) = n(r)/(4\pi r^2 \varrho \delta r). \tag{19}$$

where δr is the radial increment for $n(r)$; $n(r)$ is the number of particles found on average within $r - \delta r/2 \leqslant r \leqslant r + \delta r/2$. An example for $P_e = 5$ and $\mu_y = 4$ is shown in Figure 11. The field causes the first coordination shell to move in. The first

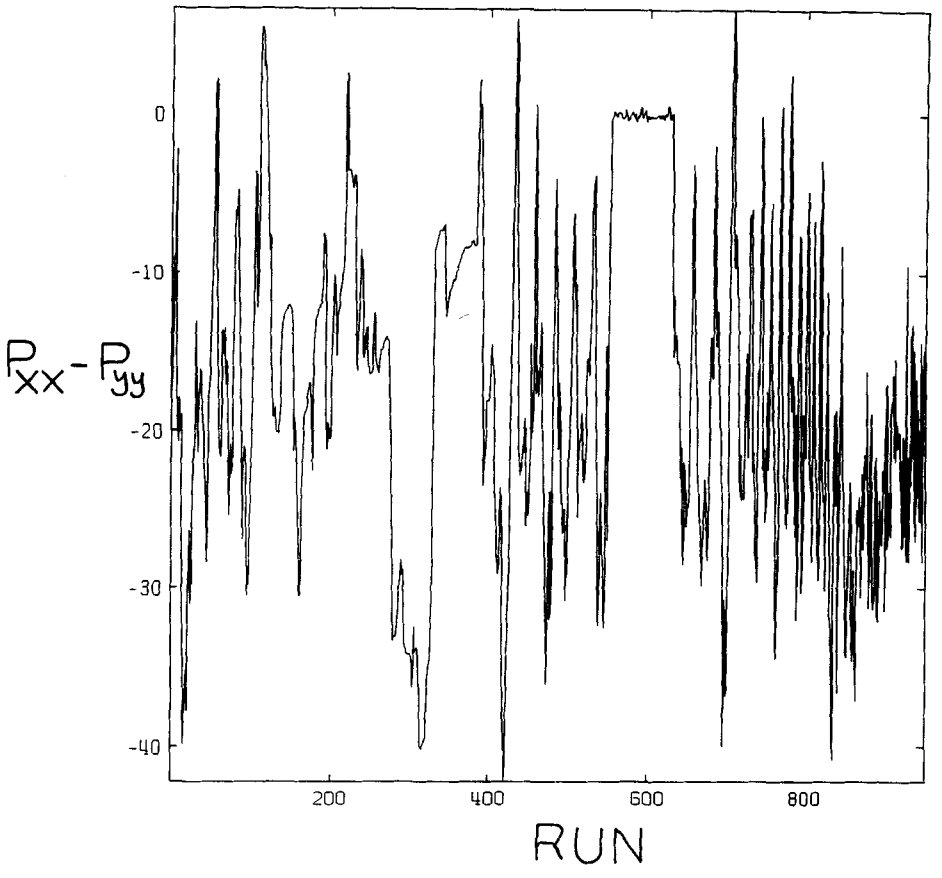

Figure 4 As for Figure 2 except the pressure difference, $P_{xx} - P_{yy}$, is given over the same sequence.

peak is at r = 1.0 in the E → 0 limit. A partial resolution of this function into x, y and z components is indicated by the function, $g_{\alpha\alpha}(r)$ where $\alpha = x, y$ or z,

$$g_{\alpha\alpha}(r) = n_{\alpha\alpha}(r)/(4\pi r^2 \varrho \delta r), \tag{20}$$

where $n_{\alpha\alpha}(r)$ is the average of $r_{\alpha ij}^2/r_{ij}^2$ particles found within $r - \delta r/2 \leqslant r \leqslant r + \delta r/2$. In Figure 12 we show $g_{xx}(r)$, $g_{yy}(r)$ and g_{zz} for a typical field-on sheared state ($P_e = 4$). The dipolar field is seen to cause local ordering of particles in the y direction with a sharp peak at $r \sim 0.8$. The x 'structure' is characterised by a strong peak at $r \approx 1.0$. Local order, indeed the presence of particles, in the z direction has largely disappeared until $r \sim 1.5$. Therefore these functions reflect major distortions of the first coordination shell caused by the combined effects of shear and electric field.

4. CONCLUSIONS

In this report we present the first simulations of the electro-rheological effect. The

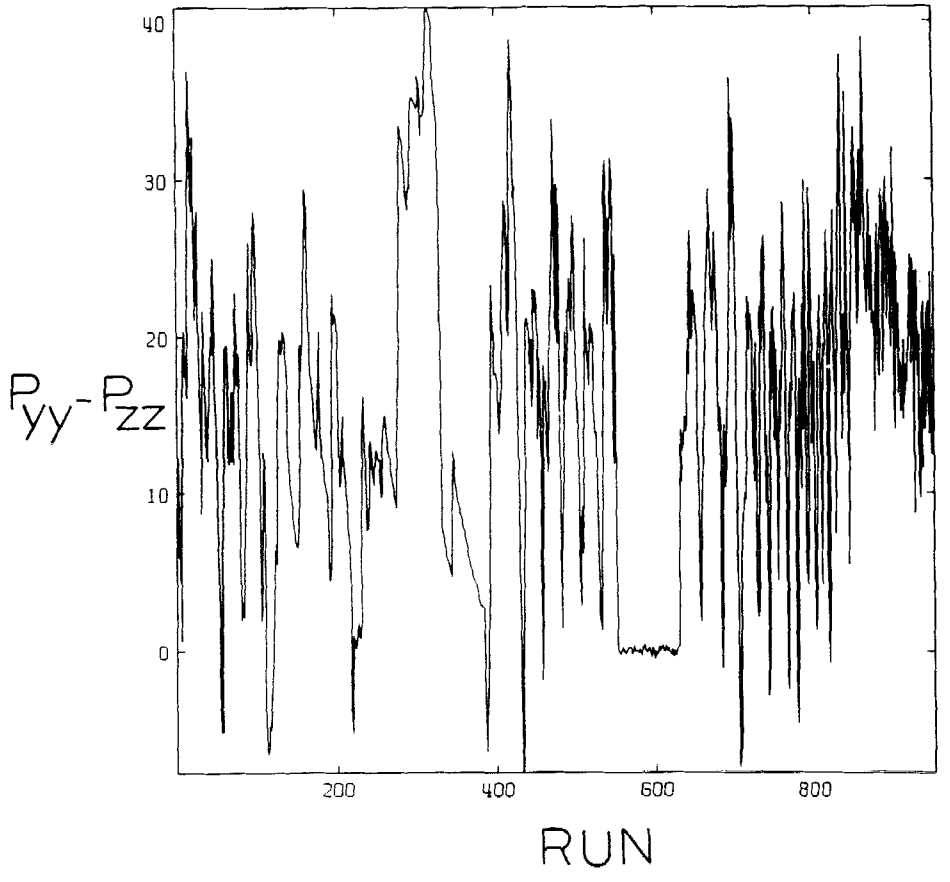

Figure 5 As for Figure 2 except the pressure difference, $P_{yy} - P_{zz}$, is given over the same sequence.

simulated structures and viscosity changes on application of the field in a form that agrees well with the experimental evidence. Strings of particles line up along the applied electric field, perpendicular to the shearing plates (which also serve as the electrodes). These resist shear flow as the shear flow tilts them and, as these macro-particles are the stress carrying components of the suspension, the strings enhance the viscosity.

The electro-rheological effect takes place on a *m*s time scale. The natural structural relaxation times for the particles employed (of the size 75 μm) are in excess of $\sim 10^4$ s. Therefore Brownian motion is incapable of forming the strings in the observed time scale. In fact, the particles move about 10^7 too slowly. Consequently we suggest that Brownian diffusion plays no significant part in this effect, the drift of the particles due to the electric field and the colloid–colloid particle interactions alone being responsible for all essential structural changes. Having simulated the electro-rheological effect to a promising extent, we are currently investigating those parameters that optimise the effect.

Although the present model is extremely successful in uncovering the microscopic origins of the ER effect its limitations are worth repeating. The applied electric field

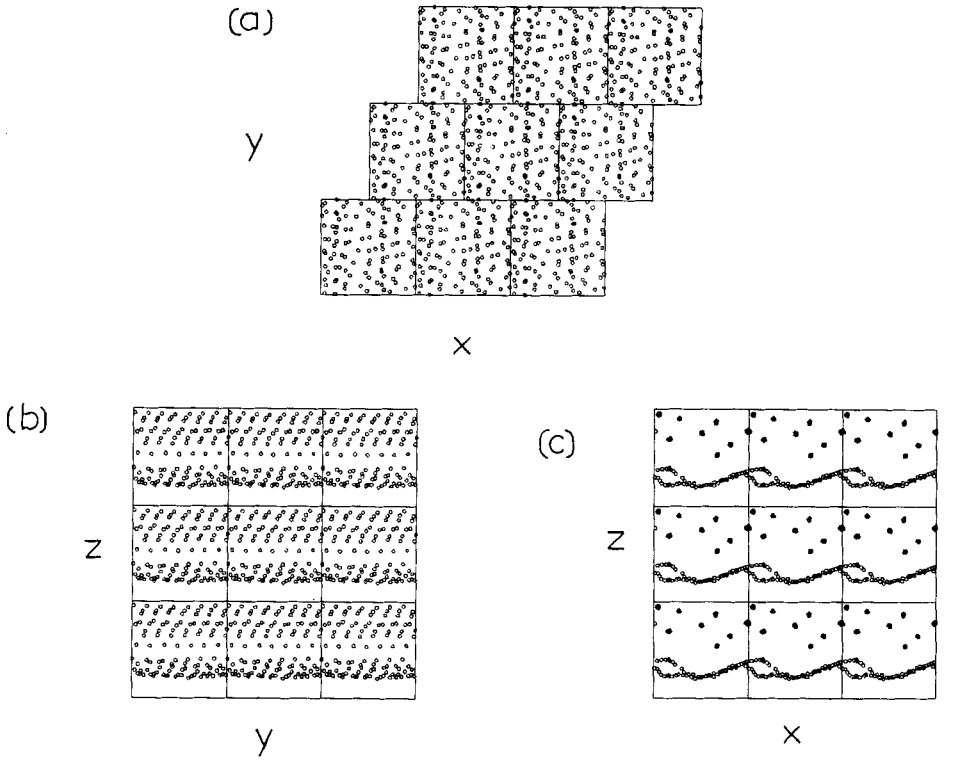

Figure 6 Projections of the model colloid particle centres on planes. All N = 108 particles are given at a reduced radius of 0.1 σ to assist the presentation. The central square is the real BD cell. The surrounding 8 squares are the image cells, appropriatly shifted with Lees-Edwards boundary conditions in the xy plane. The streaming velocity is in the x direction. The velocity gradient is in the y direction. P_e = 0.02 and μ_y = 4.

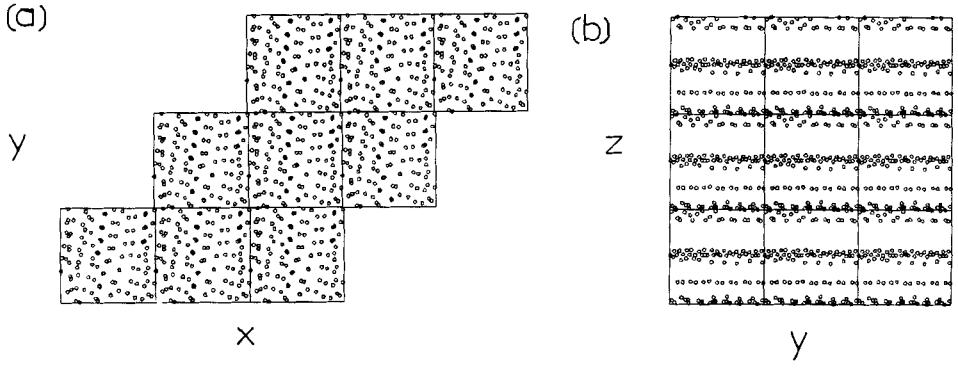

Figure 7 As for Figure 6, except that P_e = 0.05 and μ_y = 4.

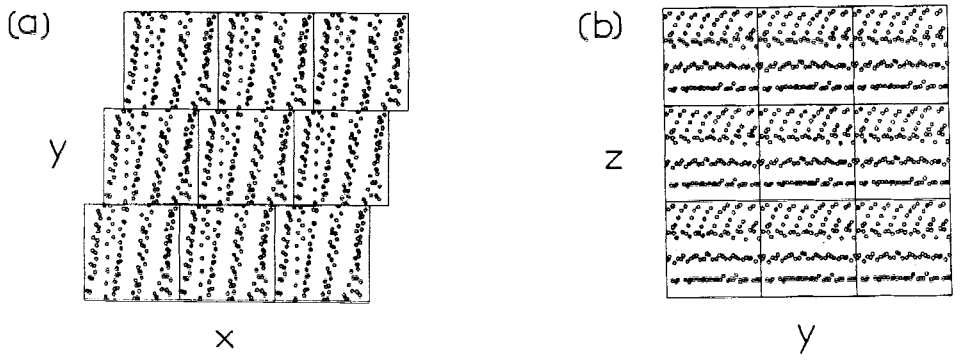

Figure 8 As for Figure 6, except that $P_e = 0.2$ and $\mu_y = 4$.

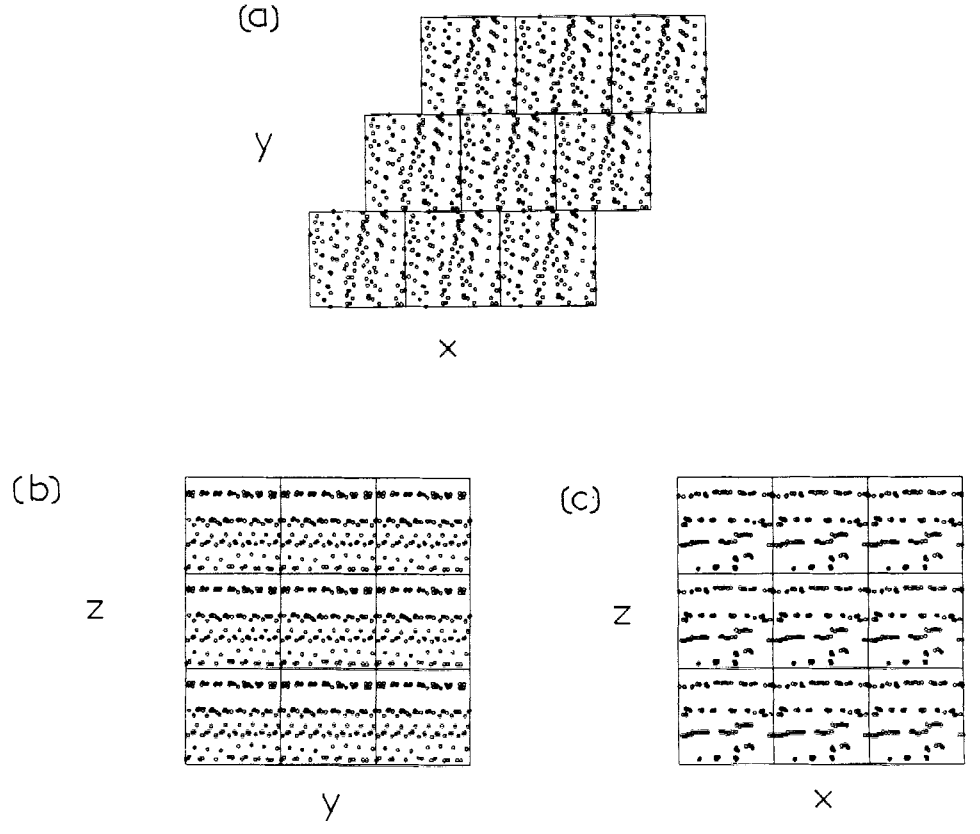

Figure 9 As for Figure 6, except that $P_e = 0.4$ and $\mu_y = 4$.

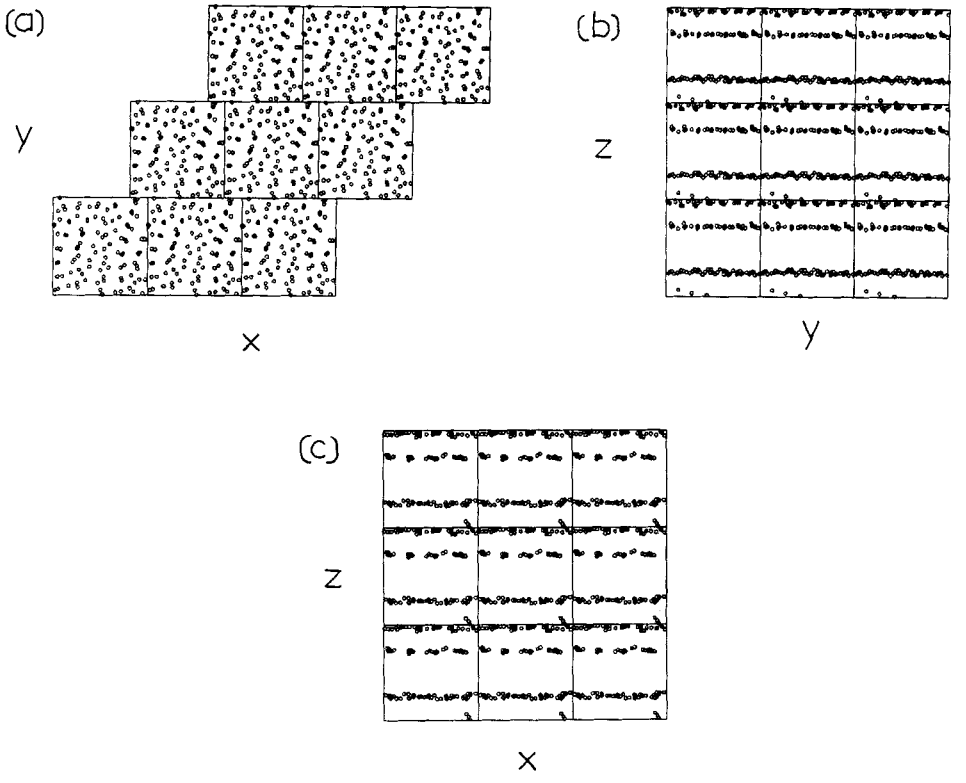

Figure 10 As for Figure 6, except that $P_e = 5$ and $\mu_y = 4$.

enters this model by inducing point dipoles on the colloidal particles. A more realistic representation of the actual charge redistribution caused by the electric field awaits further experimental work. The colloidal dynamics are modelled using the Langevin equation. This is an inadequate representation of the hydrodynamic-related interactions between the solid particles. It causes the collisions between the particles to be too fierce. This failing should be corrected when the relevant advances in methodology become available.

Acknowledgements

D.M.H. gratefully thanks The Royal Society for the award of a Royal Society 1983 University Research Fellowship. P.B. thanks Castrol (Pangbourne) and the S.E.R.C. for the award of a C.A.S.E. studentship. D.G.G. and L.H.S. thank Castrol for supporting the experimental programme on electro-rheology.

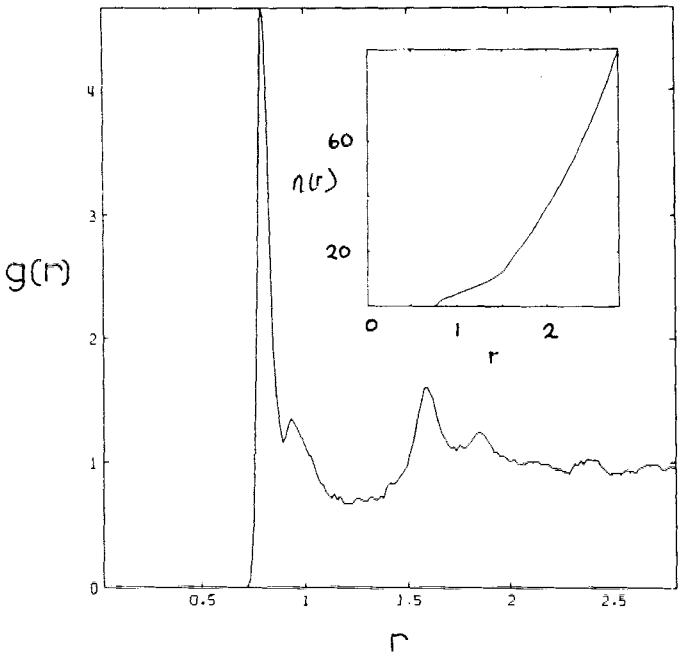

Figure 11 The pair radial distribution function, $g(r)$, for the state of figure 10. The insert is the integrated coordination number.

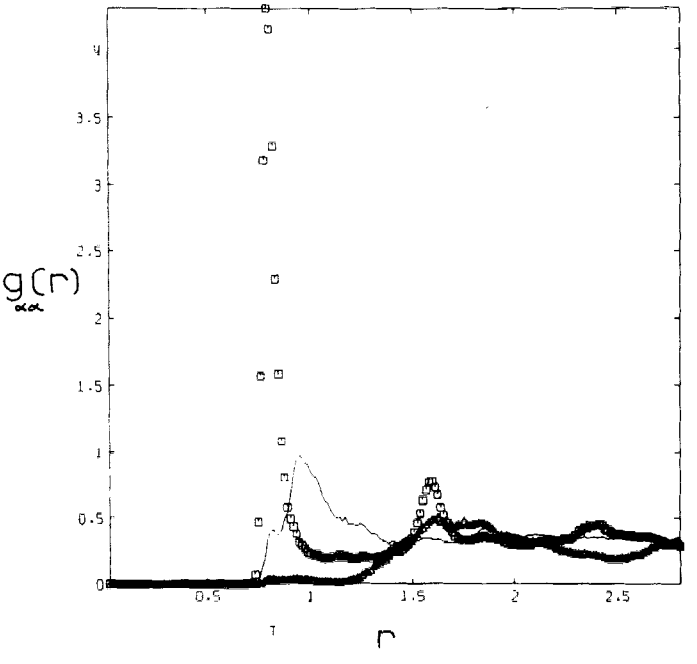

Figure 12 The functions q_{xx} (solid line), g_{yy} (squares), and g_{zz} (triangles) for the state of Figure 11.

References

[1] W.M. Winslow, "Induced fibration of suspensions," *J. Appl. Phys.*, **20,** 1137 (1949).

[2] A.F. Sprecher, J.D. Carlson and H. Conrad, "Electrorheology at small strains and strain rates of suspensions of silica particles in silicone oil," *Mater, Science and Engineering,* **95,** 187 (1987).

[3] D.L. Klass and T.W. Martinek, "Electroviscous fluids. I. rheological properties," *J. Appl. Phys.*, **38,** 67 (1967).

[4] D.L. Klass and T.W. Martinek, "Electroviscous fluids. II. electrical properties," *J. Appl. Phys.*, **38,** 75 (1967).

[5] H. Block, K.M.W. Goodwin, E.M. Gregson and S.M. Walker, "Stimulated resonance between electrical and shear fields by a colloid system," *Nature*, **275,** 632 (1978).

[6] P. Bailey, D.G. Gillies and L.T. Sutcliffe, unpublished experimental results.

[7] D.M. Heyes, J.J. Kim, C.J. Montrose and T.A. Litovitz, "Time dependent nonlinear shear stress effects in simple liquids: a molecular dynamics study," *J. Chem. Phys.*, **73,** 3987 (1980).

[8] D.M. Heyes, "Rheology of molecular liquids and concentrated suspensions by microscopic dynamical simulations," *J. Non-Newt. Fl. Mech.*, **27,** 47 (1988).

[9] K.D. Hammonds, and D.M. Heyes, "Transport coefficients of model simple liquids: a molecular-dynamics study and effective hard-sphere analysis," *J. Chem. Soc. Faraday Trans. 2,* **84,** 705 (1988).

[10] J.N. Cape and L.V. Woodcock, "Soft-sphere model for the crystal-liquid interface: a molecular dynamics calculation of the surface stress," *J. Chem. Phys.*, **73,** 2420 (1980).

[11] D.M. Heyes, "Shear thinning and thickening of the Lennard-Jones liquid: a molecular dynamics study," *J. Chem. Soc. Farad. Trans. 2,* **82,** 1365 (1986).

[12] P.M. Mors, R. Botet and R. Jullien, "Cluster–cluster aggregation with dipolar interactions," *J. Phys. A: Math. & General,* **20,** L975 (1987).